Dalton Transactions

Accepted Manuscript

ROYAL SOCIETY OF CHEMISTRY

www.rsc.org/dalton

Journal Name

RSCPublishing

ARTICLE

Multi-step mechanism and integrity of titanate nanoribbons

Cite this: DOI: 10.1039/x0xx00000x

Vanessa Bellat,[a] Rémi Chassagnon,[a] Olivier Heintz,[a] Lucien Saviot,[a] David Vandroux,[b] and Nadine Millot[a*]

Received 00th January 2012,
Accepted 00th January 2012

DOI: 10.1039/x0xx00000x

www.rsc.org/

A one-step hydrothermal treatment of TiO_2 powders in strongly basic conditions has been used to synthesize titanate nanoribbons. The nanoparticles were thoroughly characterized using several methods including transmission electron microscopy (TEM), X-ray diffraction (XRD), Raman spectroscopy and X-ray photoelectron spectrometry (XPS) to determine their morphological, structural and chemical characteristics. The influence of the nature and size of the TiO_2 precursor and of the reaction duration on the formation of the nanoribbons was investigated. The conditions required to obtain only titanate nanoribbons with a width from 100 to 200 nm and several tens of micrometers in length were determined: the optimum precursor's grain size is about 25 nm and the reaction duration should be at least 20h. Starting from our experimental results, we propose a multi-step mechanism of formation. In addition, a study of the integrity of the titanate nanoribbons structure reveals that they are made of an assembly of smaller ribbons juxtaposed and piled up on top of one another.

Introduction

Since the observation of carbon nanotubes by Iijima in 1991 [1], nanotubes [2-5] and especially those derived from titanium oxides [6-9] have been thoroughly studied. The pioneering work on titanium oxides nanotubes was reported by Kasuga *et al.* in 1998 [10]. The synthesis was achieved using a hydrothermal treatment in strongly basic conditions and a nanosize TiO_2 precursor. Many works describe the synthesis of titanium oxide nanotubes using different physical chemistry processes [11-15], their characterization and their numerous applications in various fields [16-20]. On the other hand, other 1-dimensional morphologies such as nanowires and 2-dimensional morphologies such as nanoribbons and nanosheets have attracted less attention. Those nanostructures and especially nanoribbons were mostly considered as undesired by-products or as an intermediate step of the nanotube formation [21]. But during the last ten years, their morphologic, structural and chemical properties have enabled titanium oxide nanoribbons to move out of the nanotube shadows into the limelight, becoming a full-fledged recognized nanostructure more and more studied by scientists.

Still, the different morphologies of 1- or 2-dimensional titanate nanomaterials are still debated in the literature. Nanotube morphology has been described in numerous studies [22-24] but the difference between nanowires, nanoribbons and nanosheets has still not been clearly defined. In the end, there are four different 1- or 2-dimensional morphologies for titanium oxide nanoparticles depicted in Scheme 1: nanotubes (a1 and a2), nanowires often called nanorods or nanofibers (b), nanoribbons sometimes called nanobelts (c) and nanosheets (d).

According to Bavykin *et al.* [25], each morphology presents particular distinctive features. The tubular morphology of titanates can be easily identified since they are made of multilayers (2 to 10) rolled up in a spiral with their two ends open. Their external diameter is around 10 nm and their length ranges from 100 to 200 nm (sch. 1a1). Titanium oxide nanotubes (TiO_2) synthesized by electrochemical methods are cylindrical with an inner and outer diameter. Their outer diameter usually varies from 30 to 200 nm and their length ranges from 100 nanometers to several micrometers (sch. 1a2) [26, 27].

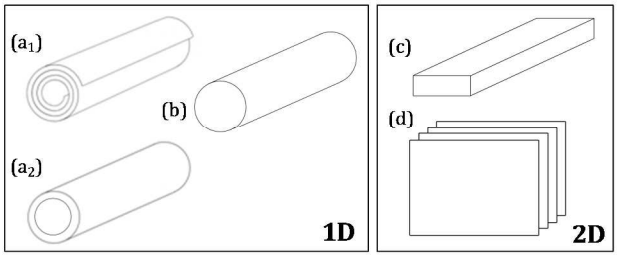

Scheme 1: Scheme of four different titanate or TiO_2 morphologies: (a_1 and a_2) nanotubes (b) nanowires, also called nanorods or nanofibers (c) nanoribbons, sometimes called nanobelts (d) nanosheets.

Nanowires, nanorods or nanofibers are solid cylinders. They do not have an internal layered structure. Their diameter is around 50 nm and the length is more than 1 µm (sch. 1b) [28-30]. Titanium oxide or titanates nanoribbons or nanobelts have one long dimension (length), one intermediate dimension (width) and one short dimension (thickness). These structures tend to have a good crystallinity and their length can reach 10 micrometers while their width typically ranges from 50 to 200 nm (sch. 1c) [29, 31, 32]. They can be found in planar as well as in curved shapes. Note that

the distinction between nanowires and nanoribbons is not made clear in many publications. Many works about the synthesis of so-called nanowires deal in reality with nanoribbons (see SI 1). Finally, nanosheets which consist of a single layer or multiple layers of titanate have a very small thickness. Their length and width measure at least 100 nm (sch. 1d). As nanoribbons, they can be found in planar or curved shapes. Nanotubes can form through the rolling up of these folding nanosheets [25].

The choice of the synthesis route (see SI 1) is very important because it affects the morphology, composition and properties of the nanostructures and consequently their applications [25, 31, 33-35]. In this work, titanate nanoribbons were synthesized *via* a hydrothermal treatment in strongly basic conditions. First of all, hydrothermal treatments are an effective method to produce titanate structures of one or two dimensions. In fact, this method can be used to prepare a large variety of nanostructures such as nanotubes [36], nanoribbons [31, 37, 38] and nanosheets [39]. Moreover, the hydrothermal treatment enables nanoparticle production on a relatively large scale [40]. This approach is also considered as the most successful synthesis for titanate nanoribbons because it is a simple, cost-effective and environmentally innocuous route [41, 42]. Titanate nanoribbons obtained by a hydrothermal process have physical and chemical properties suitable for use in numerous fields like photocatalysis [43], lithium ion batteries [44], optical applications [45], dye sensitized solar cells [46] and biosensors [47]. Finally, the hydrothermal treatment has been used to produce titanate nanotubes intended for biomedical applications [48-51]. Using this process, nanoparticles can be dispersed after chemical grafting. Considering all these parameters, the hydrothermal synthesis seems to be the most appropriate way to produce titanate nanoribbons.

In this study, the influence of two hydrothermal process parameters is discussed: the nature of the TiO_2 precursor and the reaction duration. Nanoribbons have then been fully characterized in order to determine their structure, chemical composition and morphology. These high standards of characterization pointed to a multi-step mechanism of the formation of titanate nanoribbons and allowed investigation of their structural integrity.

Experimental

Titanate nanoribbons synthesis

Titanate nanoribbons were synthesized by a hydrothermal treatment in strongly basic conditions. For this reaction, 110 mL of NaOH aqueous solution at 10 $mol.L^{-1}$ was prepared and introduced into a sealed Teflon reactor. Then 440 mg of TiO_2 precursor was added to the solution and the mixture underwent pulsed ultrasound treatment for 15 min at a power of 375 W (Sonics Vibra-Cells). This first step dispersed the TiO_2 precursor in the soda solution and initiated the reaction by creating germination sites [40]. The hydrothermal treatment took place at 180°C with an autogenic pressure, for a definite duration (4 to 36 hours) and under low mechanical stirring (150 rpm). The precipitate obtained at the end of the reaction was separated from the synthesis supernatant by a centrifugation cycle of 10 min at 10,847 g. Finally, in order to wash the powder and to reach a neutral pH, the precipitate was put in a 3.5 kDa MWCO dialysis tube for several days before being freeze-dried.

To find the appropriate synthesis conditions suitable to get only nanoribbons in the final product, several parameters were varied. First, different sizes and lattice structures of the TiO_2 precursors were considered. In the literature, all of the TiO_2 phases (except for the brookite structure) have been used to obtain titanate nanoribbons: amorphous [38], anatase [45], a mixture of rutile (20%) and anatase (80%) structures named P25 [52] and rutile [53, 54]. In this study, four different TiO_2 precursors have been used. The first two are commercial TiO_2 precursors purchased from Tioxide and Degussa (rutile and P25). They have an average grain size of 175 and 25 nm respectively (fig. 11 and tab. 2 see SI 2). The last two precursors have the anatase lattice structure and were obtained by co-precipitation. This synthesis was based on hydrolysis and condensation of titanium isopropoxide and is described elsewhere [55-57].

$$Ti(OCH(CH_3)_2)_{4\,(aq)} + 2H_2O \rightarrow TiO_{2\,(s)} + 4(CH_3)_2COH_{\,(aq)}$$

After the reaction, the amorphous powder was thermally treated for 2 hours at two different temperatures, 350°C and 470°C to obtain 5-10 nm and 10-15 nm TiO_2 anatase precursors respectively [55] (See SI 2).

To determine the impact of these TiO_2 precursors on the formation of titanium nanoribbons, four syntheses were performed exactly in the same conditions (180°C, 150 rpm, 7 bar, 20 hours). Then the influence of the reaction duration on the final product morphology was studied through eight syntheses (P25 precursor, 180°C, 150 rpm, 7 bar) which were carried out with reaction times ranging from 4 to 36 hours.

Titanate nanoribbons characterization

To determine the morphology of the synthesized nanomaterials, Transmission Electron Microscopy (TEM) observations were performed with a JEOL JEM-2100 LaB_6 microscope operating at 200 kV. To measure the chemical composition of the nanoparticles, Energy Dispersive X-ray Spectroscopy (EDS) was carried out with a Jeol JED 2300T X-ray detection system.

The morphology of nanoparticles has also been characterized by Energy-Filtered Transmission Electron Microscopy (EFTEM) using a GIF Tridiem. This Gatan's post-column energy filter was implemented on a JEOL JEM-2100F and EFTEM thickness map were obtained using the log-ratio method [58]. The first map contains the total unfiltered image intensity I_t and the second only contains the zero-loss intensity I_0. The sample thickness t is then given by the following equation with λ being the mean free path for all inelastic scattering: $t = \lambda.\ln(I_t/I_0)$.

TEM pictures at low magnification (2k) were used to estimate the proportion of synthesized nanomaterials. To do so, the contents of each square of the TEM grid were assumed to be a representative sample of the global synthesis product. Then, the area occupied by the nanoparticles was geometrically delimited and its surface was manually calculated. In this area, the surface occupied by pollutants and by-products (assumed to be spherical) was also calculated and expressed as a percentage of the overall occupied surface. This arithmetic method was applied to ten different randomly-chosen squares of the TEM grid and the results were averaged in order to improve the accuracy.

The structure of the nanoparticles was obtained using different characterization techniques. X-ray diffraction (XRD) was measured with an INEL CPS 120 diffractometer using Cu Kα radiation (λ = 1.54056 Å). The correction for instrumental broadening was determined from a standard reference material (annealed BaF_2). The determination of the peak positions and the curve fitting were performed using the profile fitting program Fityk [59]. Pseudo-Voigt peak profile analysis using the Halder-Wagner method was performed to determine the average crystallite size (the size of a region over which the diffraction is coherent).

Raman spectra were measured with an inVia Renishaw microspectrometer with the 532-nm excitation line of a doubled Nd^{3+}:YAG laser. The laser beam was focused onto a 10 μm^2 area and the power was kept below 1 mW to avoid sample heating.

Finally, nitrogen physisorption isotherms were measured with a BEL Mini apparatus. First an *in situ* desorption at 150 degrees for 3h under dynamic vacuum was performed before measuring the adsorption–desorption isotherms. Adsorption isotherms were analyzed thanks to the Belsorp software by applying the Brunauer–Emmett–Teller (BET) equation to calculate the specific surface area.

To determine the chemical composition of the synthesized nanomaterials, X-ray photoelectron spectrometry (XPS) analysis was performed with a SIA 100 Riber/Cameca apparatus and a non-monochromated Al Kα X-Ray source (energy of 1486.6 eV, accelerating voltage of 12 kV and power of 200 W). Samples were prepared by depositing the powders on a 10 × 10 × 0.5 mm^3 indium sheet and a Riber Mac 2 semi-imaging spectrometer was used with a resolution (measured from the Ag 3d5/2 line width) of 2.0 eV for global spectra and 1.3 eV for windows corresponding to selected lines. The spectrometer was used with its axis perpendicular to the surface of the sample. Preliminary analyses carried out with an aluminum source revealed interferences between the Auger titanium LMM peaks and the sodium 1s level. To bypass this problem, a magnesium source was used to quantify sodium. Photoemission peak areas were calculated after background subtraction using the CasaXPS software (version 2.2) (fig. 12 see SI 3).

Results and discussion

Influence of the grain size and structure of the TiO_2 precursor on the synthesis of titanate nanoribbons

To study the effect of the TiO_2 lattice structure and the grain size of the nanoparticles on the forming of titanate nanoribbons, four syntheses were carried out using commercial (P25 and rutile) and lab-made (5-10 nm anatase and 10-15 nm anatase) precursors. TEM observations show that in every case, the hydrothermal treatment leads to the formation of nanoribbons (fig. 1). Nevertheless the nanoribbons have different sizes depending on the TiO_2 precursor which was used. Anatase and rutile precursors lead to nanoribbons of length from 1 to several tens of micrometers and width ranging from 30 to 300 nm. Moreover, for these three syntheses, non-desired particles with a more-or-less spherical shape were formed in large quantities. Their proportion is estimated at 20% of the surface area (fig. 1a, 1b, 1d). According to localized chemical analyses (EDS), these by-products do not correspond to non-transformed TiO_2 precursor as they have exactly the same chemical composition as the titanate nanoribbons. However, they were so dense that it was not possible to determine, even at high resolution, if they are composed of strongly aggregated nanoribbons or if they are full-fledged nanostructures. On the other hand, nanoribbons synthesized from the P25 precursor have a length reaching one hundred micrometers and a width between 100 and 200 nm and they get organized into a network. It is very difficult to determine accurately the length of the synthesized nanoribbons because they often extend over more than one square of the TEM grid (60 x 60 μm^2). As previously, the nanoribbon synthesis brings with it the formation of by-products. However the proportion of these undesired nanoparticles is considerably smaller than the proportion of nanoribbons (10% of the surface area fig. 1c). In the case of the P25 precursor (Degussa), experimental conditions of the hydrothermal treatment to obtain titanate nanoribbons are in agreement with the morphological phase diagram of Morgan *et al.* [60].

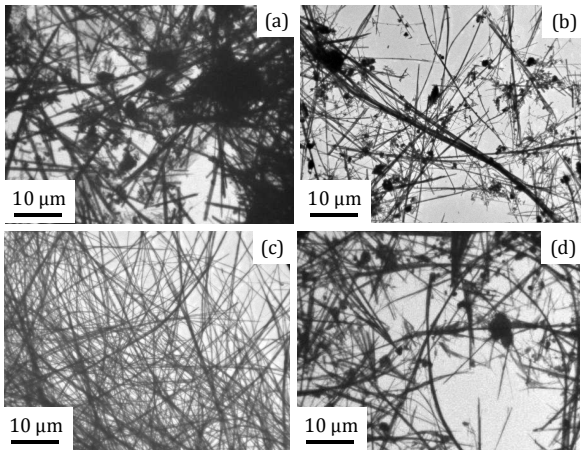

Figure 1: TEM images of nanostructures synthesized using a hydrothermal treatment and different TiO_2 precursors: (a) 5-10 nm anatase (b) 10-15 nm anatase (c) P25 and (d) rutile (440 mg TiO_2, 110 mL soda solution 10M, ultrasound treatment (30 minutes, 375 Watt), 180°C, 20 hours, 7 bar, 150 rpm).

XRD measurements reveal different signatures depending on the nature of the TiO_2 precursor. Note the absence of residual precursor (anatase and/or rutile TiO_2) for the four syntheses (fig. 2).

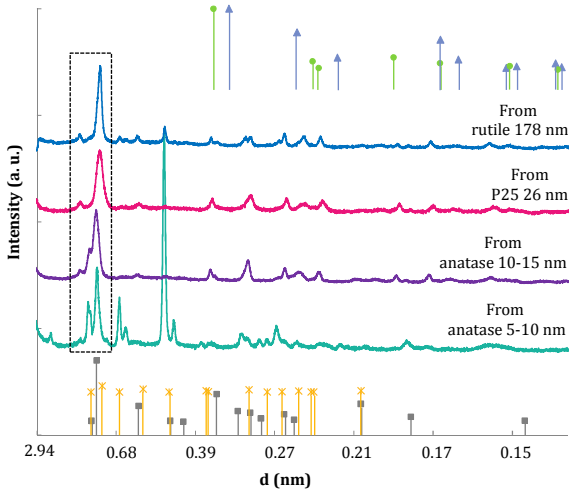

Figure 2: XRD patterns of nanoribbons synthesized by hydrothermal treatment (440 mg TiO_2, 110 mL soda solution 10M, ultrasound treatment (30 min, 375 W), 180°C, 20 hours, 7 bar, 150 rpm) from different TiO_2 precursors: 5-10 nm anatase, 10-15 nm anatase, P25 and rutile. (▲TiO_2 rutile ICDD card 72-7374, ●TiO_2 anatase ICDD card 65-5714, ■$Na_2Ti_3O_7$ ICDD card 70-9440 and ✕$H_2Ti_3O_7$ ICDD card 47-0561).

These four signatures have common features with two trititanate families. Thus some peaks can be assigned to atomic planes of $H_2Ti_3O_7$ (ICDD card 47-0561) and $Na_2Ti_3O_7$ (ICDD card 70-9440) materials (tab. 1). As nanoribbons were synthesized in the presence of a soda solution, their composition is usually defined, like in the case of nanotubes, as $Na_xH_{2-x}Ti_3O_7$ or $Na_yH_{2-y}Ti_nO_{2n+1}$, xH_2O [61].

Peak position	0.82 nm	0.57 nm	0.36 nm	0.30 nm	0.26 nm
$Na_2Ti_3O_7$	(001)	(101)	(102)	(-301)	(112)
$H_2Ti_3O_7$	(200)	(201)	(202)	(003)	(203)

Table 1: Correspondence of the characteristic peaks of nanoribbons with atomic planes of $Na_2Ti_3O_7$ (ICDD card 70-9440) and $H_2Ti_3O_7$ (ICDD card 47-0561).

Fitting the first characteristic peaks of the XRD patterns shows that they are composed of several contributions (fig. 13 see SI 4). The position of those peaks, calculated using the Bragg law are characteristic of the different nanostructures that may be obtained *i.e.*, nanoribbons, nanosheets or nanotubes. This methodology has been previously used by Papa *et al.* to quantify the heterogeneity of the products obtained during the synthesis of titanate nanotubes [22]. For the synthesis carried out from 5-10 nm anatase precursor, four peaks at d = 1.06, 0.94, 0.91 and 0.83 ± 0.01 nm are observed. The peaks around 1.06 and 0.83 nm are present for each synthesis. They respectively match nanosheets [22, 62, 63] and nanoribbons [22, 53, 64]. The area ratio of those two characteristic peaks shows that mainly nanoribbons were synthesized. When using the P25 and rutile precursors, only nanosheets and nanoribbons were formed. On the other hand, using the anatase precursors leads to a different nanostructure with inter-reticular distances around 0.90 nm. Those nanostructures could correspond to the undesired nanoparticles observed on TEM pictures. However, this hypothesis is quickly refuted. This distance is not observed when using the rutile precursor while an identical "pollution" was observed by TEM. Moreover, direct measurements on the high resolution TEM pictures and the SAED (Selected Area Electron Diffraction) analyses show that the undesired nanoparticles have inter-reticular distances equal to 0.73 and 0.36 ± 0.01 nm (fig. 14 see SI5).

XRD patterns also show the appearance of peaks which are sometimes very intense at d = 3.31, 1.86, 0.66, 0.62, 0.47, 0.45 and 0.27 ± 0.01 nm in the case of the synthesis carried out from 5-10 nm anatase precursor (fig. 2 and fig. 15 see SI6). Note that those peaks also appear when using the rutile precursor but they are much less intense (fig. 2). They are also observed when using the P25 precursor under specific reaction condition (very low mechanical stirring (50 rpm) and brutal cooling, data not shown here). At this stage, several hypotheses are conceivable to explain this observation:

- appearance of a new phase: according to the ICDD database, the most intense peak at d = 0.47 ± 0.01 nm and the peak at d = 0.27 ± 0.01 nm may correspond to $Na_4Ti_3O_8$ (ICDD card 38-730). However this card is not indexed and is empty for inter-reticular distances larger than 0.54 nm (low 2θ). Moreover, it cannot explain the appearance of the other peaks. This first possibility is not sufficient to explain all the observations unless a new crystalline order which is not identified in ICDD database is considered.

- formation of a super-structure: the presence of peaks at small diffraction angles (d = 3.31 and 1.86 ± 0.01 nm) (fig. 15 see SI6) pleads for this hypothesis [65]. It may come from an ordered arrangement of the Na^+ and H^+ ions. According to the Bragg law, the peak at d = 0.66 ± 0.01 nm (2θ = 13.39°) would be the fifth-order harmonic of the peak at d = 3.31 ± 0.01 nm (2θ = 2.67°) and the one at d = 0.62 ± 0.01 nm would be the third-order harmonic of the peak at d = 1.86 ± 0.01 nm (fig. 15 and tab. 3 see SI6). Finally, the peaks at d = 0.94 and 0.91 ± 0.01 nm and their second-order harmonics at d = 0.47 and 0.45 ± 0.01 nm would match other planes of the structure.

- texturing: considering the morphology of the synthesized nanoparticles and the preparation of the XRD samples, a texturing phenomenon, matching a preferential orientation of crystals, could explain the observed spectacular variations of intensity [65].

- stack defects: the organization of those nanostructures in layers and their complex chemical composition which is not clearly determined, stack defects leading to slight shifts of diffraction peaks can be considered [65].

Given the complexity of the material, a combination of all these hypotheses seems the most likely explanation of these particular XRD patterns of nanoparticles synthesized from 5-10 nm anatase TiO_2 precursor.

Further analysis carried out by Raman spectroscopy supports the results obtained by XRD (fig. 3). Whatever the nature of the TiO_2 precursor, the shape of the four spectra is rather similar. The presence of nanoribbons is indicated by several peaks at 162, 197, 210, 239, 268, 283, 330, 380, 430, 467, 603 and 674 cm^{-1}. The first two peaks are strongly characteristic of the ribbon morphology since they are not observed for other titanate nanostructures such as nanotubes [22]. According to the literature, the Raman spectrum of $Na_2Ti_3O_7$ has characteristic peaks assigned to the stretching vibration of Ti-O-Na bonds at 280 and 372 cm^{-1} and a peak assigned to Ti-O-Ti bonds stretching vibrations of TiO_6 octahedrons at 672 cm^{-1} [66, 67]. The presence of these peaks is an indication that the structure of the nanoparticles synthesized by the hydrothermal treatment is close to that of $Na_xH_{2-x}Ti_3O_7$ tri-titanate. The spectra of nanoribbons synthesized from the P25 and rutile precursors are similar. On the other hand, when using the anatase precursors, a peak appears between 310 and 320 cm^{-1} and peaks around 430 and 475 cm^{-1} are more intense. Finally, in the case of nanoribbons synthesized from 10-15 nm anatase nanoparticles, an additional peak appears at around 250 cm^{-1}. Understanding all these results is extremely challenging. But the observed variations result in structural changes in the nanoribbons which depend on the nature and the size of the TiO_2 precursor grains used for synthesis. These variations are especially marked in the case of the TiO_2 crystallites with a size smaller than 25 nm. The presence of a super-structure (hypothesized from the XRD measurements) for the sample obtained from the 5-10 nm anatase precursor should result in narrower peaks and even in additional peaks [68]. Such peaks were not observed in this study.

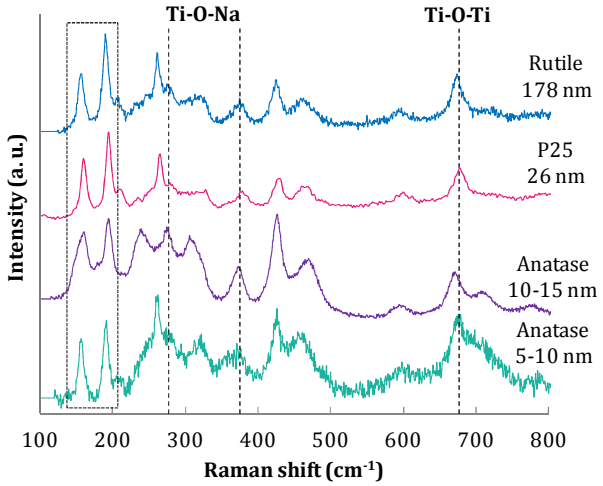

Figure 3: Raman spectra of nanoribbons synthesized by a hydrothermal treatment (440 mg TiO_2, 110 mL soda solution 10M, ultrasound treatment (30 min, 375 W), 180°C, 20 hours, 7 bar, 150 rpm) from different TiO_2 precursors: 5-10 nm anatase, 10-15 nm anatase, P25 and rutile.

The chemical composition of the synthesis products was investigated by XPS analysis. It depends on the TiO_2 precursor used during the

hydrothermal treatment (tab. 4 see SI7). First of all, it is important to emphasize that XPS which is classically considered as a surface analysis method can usually be considered as a global analysis method in the case of very thin nanostructures such as nanotubes and nanoribbons (thickness < 10 nm). In the case of nanoribbons synthesized from 5-10 nm anatase, the oxygen ratio is almost three times more than the titanium content. This low amount of titanium in the nanoribbon composition is consistent with analysis by inductively-coupled plasma atomic emission spectroscopy (ICP-AES) which showed that the synthesis supernatant had a titanium content of 0.139 $mg.L^{-1}$. This proportion is almost twice as high as the titanium content of other synthesis supernatants. On the other hand, the chemical composition of the nanoribbons synthesized from the 10-15 nm anatase, P25 and rutile precursors are identical. This result is not surprising since the nanoribbons already have a similar morphology and structure according to TEM, XRD and Raman analyses. A curve fitting of the carbon and oxygen 1s peaks shows that the carbon atoms contribute to C-C pollutions and C-O and C=O functions in a similar way for all syntheses (fig. 12 and tab. 4 see SI3 and SI7). Oxygen atoms contributing to structure oxygen, hydroxyl group and structure water are also very similar whatever the nature of the TiO_2 precursor. Nevertheless, it should be noted that the oxygen content and the proportion of C-C/C-H and C-O bonds are larger when using the 5-10 nm anatase precursor. This difference is related either to the different crystalline structures observed by XRD for nanoribbons stemming from this precursor, or to the presence of thinner nanoribbons in which case the XPS analysis is a global analysis, or to a higher proportion of organic pollution resulting from the thermal treatment of the TiO_2 precursor at a weaker temperature (tab. 2 see SI2).

When the grain size of the TiO_2 precursor is larger than 10 nm, very similar nanostructures and chemical compositions are obtained. However using the P25 precursor results in a larger amount of titanate nanoribbons. When using this precursor, nanoribbons have homogenous dimensions (width ranging from 100 to 200 nm and length reaching 100 µm), the by-product proportion does not exceed 10% and their composition as well as that of the nanoribbons can be written as $Na_yH_{2-y}Ti_nO_{2n+1}$, xH_2O.

Influence of the reaction time: toward a mechanism for the formation of the nanoribbons.

According to the literature, the hydrothermal treatment duration is a key parameter to control the morphology [69-71]. TEM observations show that after 1 hour, the hydrothermal treatment leads to the formation of titanate nanosheets (fig. 4a). Nanotubes are also present in a large amount. Their proportion reaches 40% of the surface area. However their formation is incomplete as revealed by their heterogeneous dimensions and their variable number of walls (fig. 4b). The presence of such nanotubes after one hour of hydrothermal treatment suggests that the transformation of TiO_2 grains into titanate nanosheets requires less than one hour of reaction.

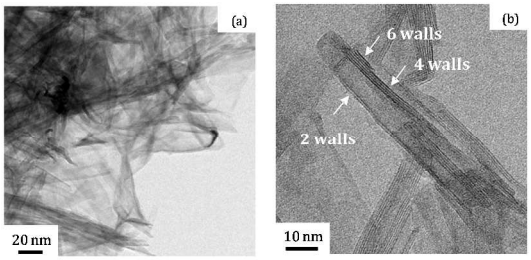

Figure 4: TEM pictures of (a) titanate nanosheets and (b) nanotubes after one hour of hydrothermal treatment (440 mg P25 TiO_2 precursor, 110 mL soda solution 10M, ultrasound treatment (30 min, 375 W), 180°C, 7 bar, 150 rpm).

After 4 hours of hydrothermal treatment, the synthesis leads to the forming of nanotubes (fig. 5). Their length ranges from 50 to 200 nm and their external diameter reaches 10 nm. Contrary to what was reported in the literature [72], some very thin nanoribbons having a width around 50 nm are present in the synthesis product but their proportion is very low (less than 10% of the surface area). After 8 hours of reaction, the tubular morphology is still dominant (fig. 5). Nevertheless the proportion of nanoribbons increases and exceeds 30% of the surface area. Moreover the size of the nanoribbons is larger. Their width reaches 150 nm. After 12 hours of treatment, nanoribbons are the main product of the reaction (fig. 5). They vary in size with widths from 50 to 200 nm and lengths from 500 nm to several micrometers. Some nanotubes are still observed but their proportion does not exceed 20%. For durations from 16 to 36 hours, only nanoribbons are observed (fig. 5). Their length varies from several micrometers to tens of micrometers and their width ranges from 50 to 200 nm. For durations of 20 and 24 hours, the size of the nanoribbons becomes nearly uniform. Their width only varies from 100 to 200 nm and their length reaches several tens of micrometers. For 28 and 36 hours of duration, the length is similar but the width increases since it varies from 100 to 600 nm. This increase is explained by the fact that nanoribbons tend to juxtapose each other to form larger entities.

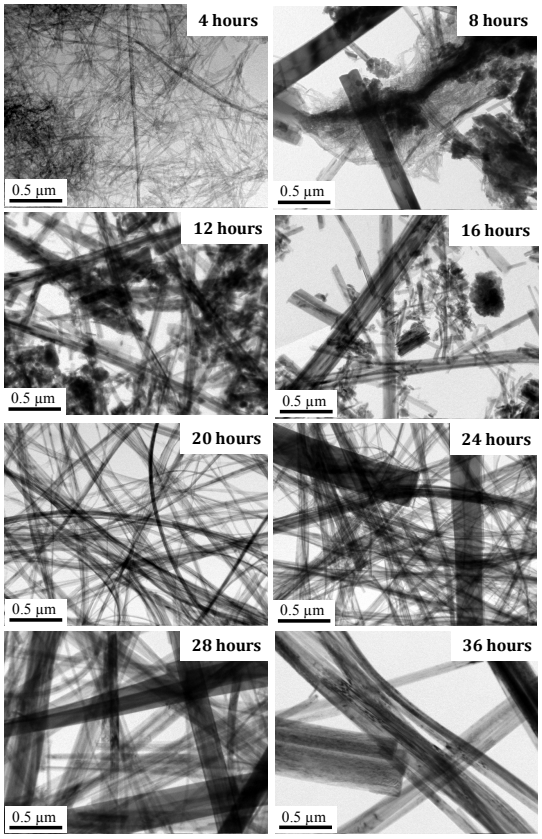

Figure 5: TEM micrographs of nanoparticles synthesized by a hydrothermal treatment (440 mg P25 TiO_2 precursor, 110 mL soda solution 10M, ultrasound treatment (30 min, 375 W), 180°C, 7 bar, 150 rpm) for different reaction times varying from 4 to 36 hours.

The results of XRD and Raman spectroscopy analysis are very difficult to interpret. Nevertheless, they support some points highlighted by TEM observations. For 4 hours of reaction, the XRD pattern matches the nanotube's signature as the four characteristic peaks of the tubular morphology are visible (d = 0.94, 0.37, 0.32 and 0.19 ± 0.01 nm) (fig. 6a) [22, 40]. Similarly, the Raman spectrum

shows characteristic peaks position at 283, 451 and 700 cm^{-1} which match the nanotube's signature (fig. 6b) [73]. For 8 to 16 hours of reaction, even if the TEM observations show that the product is composed of a mixture of nanotubes and nanoribbons, the nanoribbon's signature is the only one observed in the XRD and Raman measurements (fig. 6a and 6b). This can be explained by the fact that the nanotube's signature is composed of broad and weak peaks illustrating a faintly-ordered structure resulting from the irregular rolling up of nanosheets. On the other hand, nanoribbons exhibit thin and intense peaks related to their ordered and homogeneous structure. Nevertheless, between 8 and 16 hours of reaction, the characteristic peaks of the nanoribbons are not clearly defined and the change of the shape of the peaks is noteworthy. This suggests that the nanoribbon structure changes because their growth is not complete. For more than 20 hours of reaction, the XRD and Raman signatures of the nanoribbons is composed of well-defined peaks whose position and shape do not change up to 36 hours of reaction (fig. 6a and 6b). Thus we conclude that a minimum time of 20 hours is required to synthesize titanate nanoribbons.

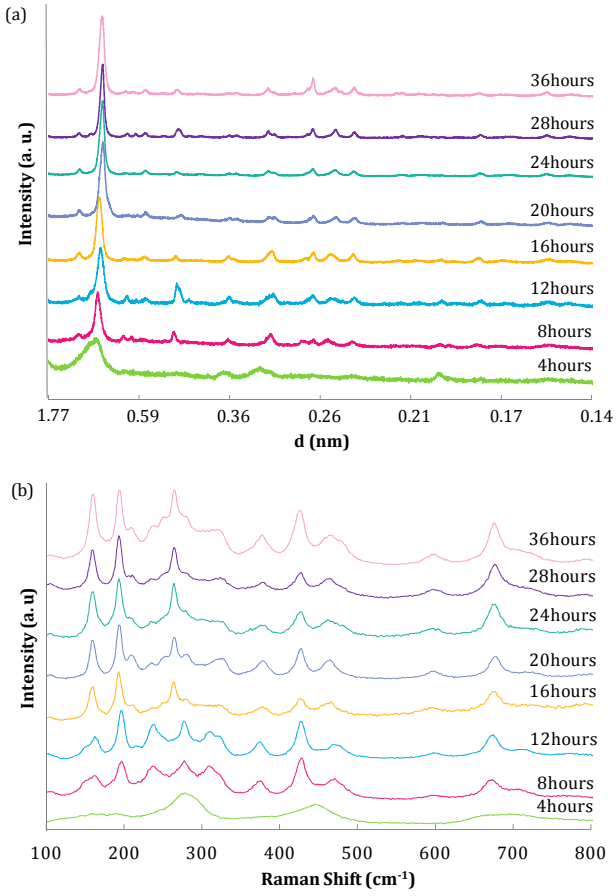

Figure 6: (a) XRD patterns and (b) Raman spectra of nanoparticles synthesized by an hydrothermal treatment (440 mg P25 TiO_2 precursor, 110 mL soda solution 10M, ultrasound treatment (30 min, 375 W), 180°C, 7 bar, 150 rpm) for different reaction times varying from 4 to 36 hours.

Despite the large differences in their morphology and structure, the nanoparticles synthesized between 4 and 36 hours have a similar overall chemical composition according to XPS analysis. The carbon, oxygen and titanium proportions remain constant (respectively around 22, 57 and 14 ± 1%) whatever the duration of the hydrothermal treatment (data not shown here). The sodium ratio is the only one which decreases with increasing durations (from 9 to 4 ± 1%). Moreover, fitting the oxygen 1s level shows that the O^{2-} component increases for 28 and 36 hours of reaction from 34 to 45 ± 10%.

All these observations reveal that there are significant morphological and structural changes during the hydrothermal treatment. To explain these results, a multi-step mechanism for the formation of titanate nanoribbons is proposed in the following. Until 1 hour of reaction, the TiO_2 precursor reacts with the alkaline solution. This leads to the formation of sodium titanate nanosheets. Then, between 1 and 4 hours, due to the chemical environment, those sheets roll up to form $Na_xH_{2-x}Ti_3O_7$ nanotubes [74, 75]. The nanosheet formation and the roll-up mechanism explaining the forming of nanotubes are widely described in the literature [74]. According to Yuan *et al.* and Chen *et al.*, when immersed in a basic solution with a temperature between 100 and 160°C, some Ti-O-Ti bonds at the surface of the titanium oxide raw material react with the hydroxide ions to form nanosheets composed of octahedral TiO_6 units [29, 76]. For higher temperatures (180°C), the number of unsaturated dangling bonds at the surface of the nanosheets increases. To saturate these bonds and reduce the surface-to-volume ratio, the sheets roll up, lowering the total energy and leading to the forming of nanotubes [24, 38, 74, 77].

The process leading to the conversion of nanotubes into nanoribbons was rarely studied. This conversion can be achieved by the unzipping of the nanotubes followed by a crystalline growth. A similar phenomenon leading to the transformation of graphene nanotubes into nanoribbons was explained by oxidation and intercalation reactions [80, 81]. But the increase of the amount of O^{2-} measured by XPS analyses is not large enough to sustain the hypothesis of the unzipping of nanotubes by an oxidation reaction. According to Horvath *et al.* and Sheng *et al.*, the conversion of nanotubes into nanoribbons is a process under thermodynamic control [70, 80]. In order to reduce the surface free enthalpy, nanotubes sharing a common crystallographic orientation with an unsaturated titanium-oxygen bond or hydrogen-oxygen bonds assemble together by oxolation or olation. This spontaneous self-assembly is achieved through the dissolution of sodium trititanate from the weakest parts of the nanotube (presumably the tube ends) followed by a recrystallization process within the nanotube channels to yield solid nanoribbons [70, 76]. Another hypothesis was suggested by Elsanousi *et al.* The transition from the tubes to the ribbons is explained by Ostwald ripening. Nanotubes act as fuel for the growth of bigger nanoribbon structures [73]. Nevertheless these two theories cannot explain all the TEM, XRD and Raman results carried out in the present study. This is the reason why a new mechanism for their formation is proposed here (fig. 7).

After the formation of nanotubes by the rolling up of titanate nanosheets (fig. 4b and fig. 16a in SI8), the Ti-O-Ti bonds should break and cause the instability of the nanotubes in the alkaline solution between 8 and 12 hours of reaction. Nanotubes will split up (fig. 16b see SI8) and Ti^{4+} ions will be released into the soda solution. According to Bavykin's work [81], the presence of free titanium ions into the alkaline environment lead to the formation of $TiO_2(OH)_2^{2-}$ monotitanates. Titanium ions in solution act as nutriments for the formation and the growth of nanoribbons.

From 12 hours of reaction, nanotube fragments would gather to form Ti-O-Ti bonds. From 16 to 36 hours of reaction, the new structures, which are much more stable in the alkaline solution than nanotubes, will keep on growing to form bigger nanoribbons by the piling up of smaller ones (fig. 7).

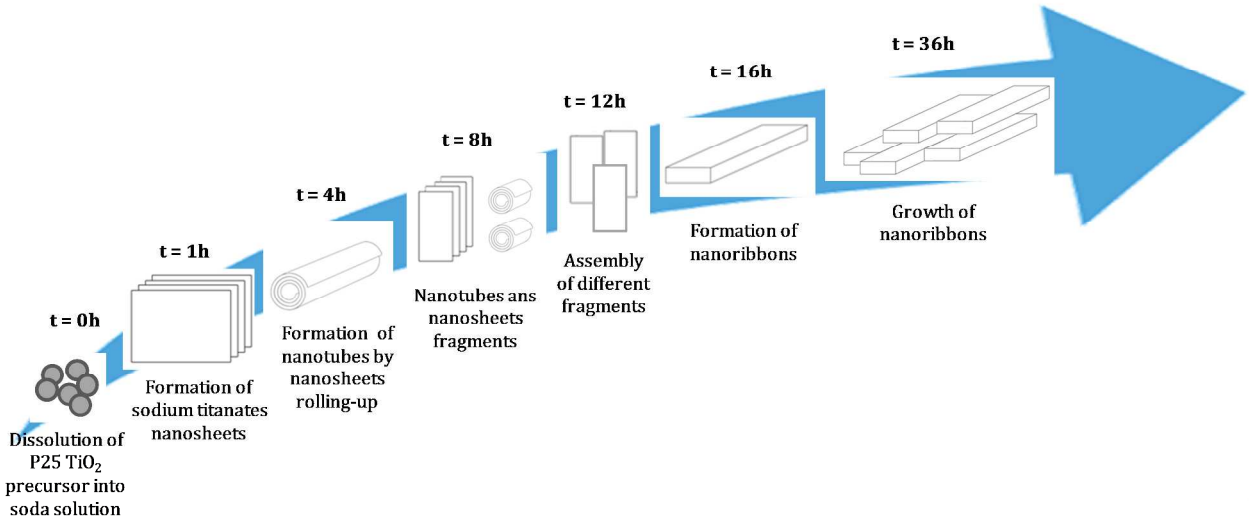

Figure 7: Scheme of the forming mechanism of titanate nanoribbons illustrating the significant morphological and structural evolution during the hydrothermal treatment.

Integrity of titanate nanoribbons

To the best of our knowledge, there is no information in the literature concerning the integrity of titanate nanoribbons. According to the forming mechanisms previously proposed (fig. 7), titanate nanoribbons are super-structures composed of an assembly of ribbons with lower dimensions juxtaposed and superimposed over one another. TEM observations enable us to study the changes in the structure of the nanoribbons after different ultrasound treatments (bath and stick (750W), fig. 8).

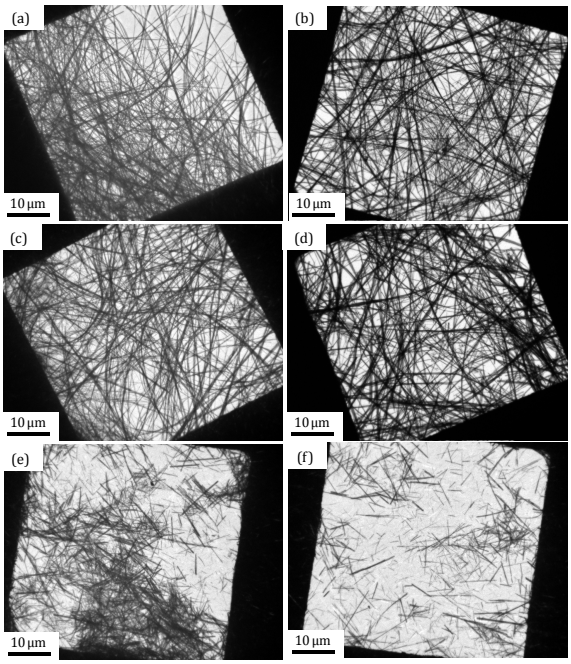

Figure 8: TEM pictures of titanates nanoribbons (a) in powder form and dispersed into deionised water (1 mg.mL^{-1}) by (b) vibrating table (c) manual shaking (d) magnetic stirring (e) ultrasound bath and (f) ultrasound stick.

Titanate nanoribbons in suspension in deionised water (1 mg.mL^{-1}) and dispersed for 1 min by vibrations (300 tremors.min^{-1}), manual shaking or magnetic stirring (300 rpm) (fig. 8a to 8d) have lengths still reaching several tens of micrometers and widths still between 100 and 200 nm. When observed after the ultrasound treatments (fig. 8e and 8f), their length varies from 500 nm to 15 µm and most of them (80%) have a width less than 150 nm.

At this stage, two hypotheses are plausible:

- Possibly nanoribbons are fragile and tend to break and tear when exposed to ultrasound. Some TEM images may back up this hypothesis (fig. 17 see SI9). But the thickness of the nanoribbons is rather large making this breaking up under ultrasound unlikely. Moreover, the duration of the treatment and the ultrasound power are not sufficient to deteriorate the oxide-based structure composed of strong iono-covalent bonds.

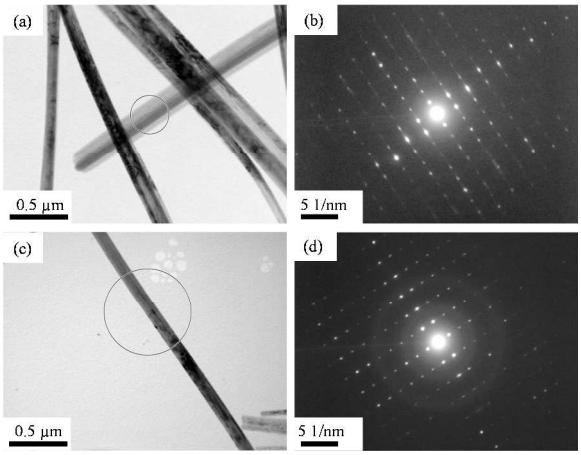

Figure 9: TEM pictures and SAED images of titanate nanoribbons dispersed (a-b) without sonication and (c-d) by ultrasound treatment (1 min, 375 W).

- Or else possibly the assembly of ribbons with variable dimensions forming the structure of titanate nanoribbons is destroyed by the applied ultrasound. SAED analysis carried out on a titanate nanoribbon dispersed by manual agitation and on one sample dispersed by ultrasound supports this theory. The diffraction patterns of manually dispersed (fig. 9b) and sonicated (fig. 9d) nanoribbons are almost the same. The only differences are the streaks around

diffraction spots in the diffraction pattern of the manually dispersed nanoribbons. These streaks could be indicators of the presence of a super-structure, of very small texturation, of stacks defects or a combination of all of these.

This study of the integrity of titanate nanoribbons highlights their particular morphology. TEM observations and SAED analyses confirm that titanate nanoribbons are in fact super-structures whose architecture is an agglomeration of several ribbons with variable dimensions which tends to deagglomerate when exposed to ultrasound (sch. 2).

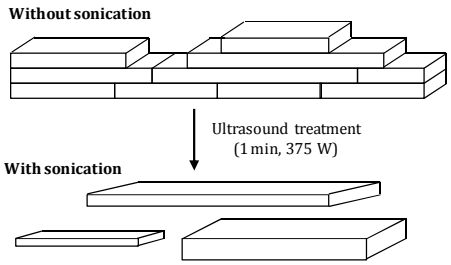

Scheme 2: Scheme illustrating the breakup of the assembly of ribbons forming the titanate super-structure under the ultrasound treatment.

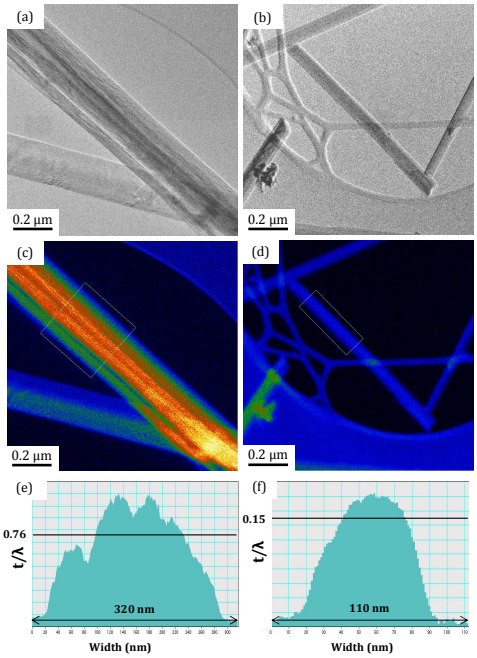

Figure 10: (a-b) TEM pictures, (c-d) thickness maps in EFTEM and (e-f) relative thickness line profiles of titanate nanoribbons dispersed (a-c-e) without sonication and (b-d-f) by ultrasound treatment (1 min, 375 W).

A final analysis technique was used to provide additional evidence on the nanoribbon morphology: a combination of Electron Energy Loss Spectroscopy (EELS) and EFTEM. The aim of this experiment was not the determination of the absolute thickness t but rather the acquisition of relative t/λ thickness maps exhibiting the thickness variations of the nanoribbons. TEM micrographs and EFTEM thickness maps were obtained for a raw sample (fig. 10a, 10c) and for a sample exposed to the ultrasonic stick (fig. 10b, 10d). The corresponding integrated line profiles (fig. 10e and 10f) over the region of interest (white rectangles) exhibit the relative thickness value. Fig 10e points out the fluctuation (mean deviation 0.21) and large value of the relative thickness in the case of the raw material: color variation from blue to yellow in fig. 10c. It also highlights the consistency (mean deviation 0.03) and the relative thickness low value of 0.15 in the case of the sonicated nanoribbons: consistency is revealed by the color uniformity, nearly only blue color (fig. 10d). All these results support the structural morphology evolution of the previous schematic figure (sch. 2).

Conclusions

To synthesize titanate nanoribbons by the hydrothermal treatment of a pulverulent TiO_2 precursor in strongly basic conditions, it is essential to master the reaction parameters in order to control the morphological, structural and chemical characteristics. In this work, the influence of two synthesis parameters on the formation of nanoribbons was assessed. The results of this study shows that to obtain titanate nanoribbons with widths from 100 to 200 nm, a length reaching several tens micrometers and having a crystalline structure and composition close to those of $Na_yH_{2-y}Ti_nO_{2n+1}$, xH_2O, the use of the P25 TiO_2 precursor with a grain size around 25 nm is necessary. Even if it is possible to synthesize titanate nanoribbons with other TiO_2 precursors, using P25 permits limitation of the formation of by-products during the hydrothermal treatment (< 10% of the surface area) and avoidance of structural inhomogeneities (new crystalline phases, stack defects, super-structure, *etc.*).

A reaction time of 20 hours is also required. Increasing the reaction duration results in larger nanoribbons. The study of the influence of the reaction duration also allowed presenting a multi-step mechanism of the formation of nanoribbons by the hydrothermal route. In this formation mechanism, a significant morphological and structural evolution is noteworthy. Firstly, TiO_2 grains react with the alkaline medium which leads to the formation of sodium titanate nanosheets. Then these sheets roll up to form $Na_xH_{2-x}Ti_3O_7$ nanotubes. Thereafter the tubes which are unstable in the soda solution split up and the resulting fragments gather to form nanoribbons.

Finally we report a study of the integrity of the titanate nanoribbons which shows that those nanostructures have a very special morphology. Titanate nanoribbons are super-structures composed of an assembly of ribbons with smaller sizes juxtaposed and piled up on one another.

These findings are required to develop the application of nanoribbons in various fields such as medicine, catalysis, plasmonic, lithium batteries, hydrogen storage and solar-cell technologies.

Acknowledgements

Authors acknowledge Dr. Daniel B. Murray for his careful reading of the manuscript and for helpful suggestions.

Notes and references

[a] Laboratoire Interdisciplinaire Carnot de Bourgogne (ICB), UMR 6303-CNRS Université de Bourgogne, 9 avenue Alain Savary, BP 47870, 21078 Dijon Cedex France.

[b] NVH Medicinal, Centre Hospitalier, 57 rue Vannerie, 21000 Dijon, France.

* Corresponding author nmillot@u-bourgogne.fr

Electronic Supplementary Information (ESI) available: See DOI: 10.1039/b000000x/

[1] S. Iijima, *Nature*, 1991, **354**, 56.
[2] S. H. Zhang, Z. X. Xie, Z. Y. Jiang, X. Xu, J. Xiang, R. B. Huang, L. S. Zheng, *Chem. Commun.*, 2004, **7(9)**, 1106.
[3] Z. H. Xi, Z. Q. Xue, X. D. Zhang, J. H. Song, R. M. Wang, J. Xu, Y. Song, S. L. Zhang, D. P. Yu, *Appl. Phys. Lett.*, 2003, **83(9)**, 1689.
[4] C. Wu, S. H. Yu, S. Chen, G. Liu, B. Liu, *J. Mater. Chem.*, 2006, **16**, 3326.
[5] Y. Ren, M. Niu, W. Gu, Y. Fang, *Mat. Lett.*, 2012, **82**, 148.
[6] M. A. Khan, H. T. Jung, O. B. Yang, *J. Phys. Chem. B*, 2006, **110**, 6626.
[7] G. H. Du, Q. Chen, R. C. Che, Z. Y. Yuan, L. M. Peng, *Appl. Phys. Lett.*, 2001, **79(22)**, 3702.
[8] S. Kaneco, Y. Chen, P. Westerhoff, J. C. Crittenden, *Scripta Materialia,* 2007, **56**, 373.
[9] H. H. Ou, S. L. Lo, *Sep. Purif. Tech.*, 2007, **58(1)**, 179.
[10] T. Kasuga, M. Hiramatsu, A. Hoson, T. Sekino, K. Niihara, *Langmuir*, 1998, **14(12)**, 3160.
[11] M. Zhang, Y. Bando, K. Wada, *J. Mater. Sci. Lett.*, 2001, **20**, 167.
[12] V. Gentili, S. Brutti, L. J. Hardwick, A. R. Armstrong, S. Panero, P. G. Bruce, *Chem. Mater.*, 2012, **24**, 4468.
[13] Z. Jianling, W. Xiaohui, C. Renzheng, L. Longtu, *Solid State Comm.*, 2005, **134(10)**, 705.
[14] W. Xing, J. Qi-Zhong, M. Zi-Feng, F. Min, S. Wen-Feng, *Solid State Comm.*, 2005, **136(9-10)**, 513.
[15] Y. Qiu, J. Yu, *Solid State Comm.*, 2008, **148**, 556.
[16] M. Qamar, C. R. Yoon, H. J. Oh, N. H. Lee, K. Park, D. H. Kim, K. S. Lee, W. J. Lee, S. J. Kim, *Catalysis Today*, 2008, **131(1-4)**, 3.
[17] D. V. Bavykin, A. A. Lapkin, P. K. Plucinski, J. M. Friedrich, F. C. Walsh, *J. Phys. Chem. B*, 2005, **109(41)**, 19422.
[18] D. Kuang, J. Brillet, P. Chen, M. Takata, S. Uchida, H. Miura, K. Sumioka, S. M. Zakeeruddin, M. Gratzel, *ACS Nano*, 2008, **2(6)**, 1113.
[19] M. Hosokawa, K. Nogi, M. Naito, T. U. Yokoyama, *Technology Handbook*, 2008, 521.
[20] S. Oh, S. Jin, Mater. Sci. Engin., C: *Biomim. Supramol. Sys.*, 2006, **26(8)**, 1301.
[21] W. Li, T. Fu, F. Xie, He, S. Shaofeng, *Mater. Lett.*, 2007, **61**, 730.
[22] A. L. Papa, N. Millot, L. Saviot, R. Chassagnon, O. Heintz, *J. Phys. Chem. C*, 2009, **113**, 12682.
[23] Y. F. Chen, C. Y. Lee, M. Y. Yeng, H. T. Chiu, *Mater. Chem. Phys.*, 2003, **81**, 39.
[24] W. Wang, O. K. Varghese, M. Paulose, C. A. Grimes, *J. Mater. Res.*, 2004, **19 (2)**, 417.
[25] D. V. Bavykin, J. M. Friedrich, F. C. Walsh, *Adv. Mater.*, 2006, **18**, 2807.
[26] A. Ghicov, H. Tsuchiya, J. M. Macak, P. Schmuki, *Electrochem. Com.*, 2005, **7**, 505.
[27] S. Kaneco, Y. Chen, P. Westerhoff, J. C. Crittenden, *Scri. Mater.*, 2007, **56**, 373.
[28] T. Tsumura, K. Sogabe, T. Kiyo, M. Toyoda, *Mater. Lett.*, 2011, **65**, 2322.
[29] Z. Y. Yuan, B. L. Su, *Colloids and Surfaces A: Physico-Chem. Eng. Aspects*, 2004, **241**, 173.
[30] H. Yin, G. Ding, B. Gao, F. Huang, X. Xie, M. Jiang, *Mater. Res. Bul.*, 2012, **47**, 3124.
[31] Z. Y. Yuan, J. F. Colomer, B. L. Su, *Chem. Phys. Lett.*, 2002, **363**, 362.
[32] L. Zhu, L. Cao, G. Su, W. Liu, L. Song, H. Liu, B. Dong, *Appl. Surf. Sci.*, 2011, **257**, 7932.
[33] X. Jiang, Y. Wang, T. Herricksb, Y. Xia, *Mater. Chem.*, 2004, **14**, 695.
[34] M. Wei, Y. Konishi, H. Zhou, H. Sugihara, H. Arakawa, *Chem. Phys. Lett.*, 2004, **400**, 231.
[35] Q. Yu, M. Wang, H. Chen, *Mat. Lett.*, 2010, **64**, 428.
[36] Q. Chen, W. Z. Zhou, G. H. Du, L. M. Peng, *Adv. Mater.*, 2002, **14**, 1208.
[37] A. R. Armstrong, G. Armstrong, J. Canales, P. G. Bruce, A*ngew. Chem. Int. Edit.*, 2004, **43**, 2286.
[38] D. Wu, J. Liu, X. Zhao, A. Li, Y. Chen, N. Ming, *Chem. Mater.*, 2006, **18**, 547.
[39] L. Korosi, S. Papp, E. Csapo, V. Meynen, P. Cool, I. Dekany, *Microporous Mesoporous Mater.*, 2012, **147**, 53.
[40] L. Torrente-Murciano, A. A. Lapkin, D. Chadwick, *Chem. Mater.*, 2009, **20(31)**, 6484.
[41] J. Jitputti, Y. Suzuki, S. Yoshikawa, *Catal. Com.*, 2008, **9**, 1265.
[42] B. A. Marinkovic, P. M. Jardim, E. Morgado Jr, M. A. S. de Abreu, G. T. Moure, F. Rizzo, *Mater. Res. Bulletin*, 2008, **43**, 1562.
[43] H. S. Hafez, *Mater. Lett.*, 2009, **63**, 1471.
[44] T. Beuvier, M. Richard-Plouet, M. Mancini-Le Granvalet, T. Brousse, O. Crosnier, L. Brohan, *Inorg. Chem.*, 2010, **49**, 8457.
[45] M. Feng, H. Zhan, L. Miao, *Nanotechnology*, 2010, **21**, 185707.
[46] K. Pan, Q. Zhang, Q. Wang, Z. Liu, D. Wang, J. Li, Y. Bai, *Thin Solid Films*, 2007, **515**, 4085.
[47] A. Liu, *Biosens. Bioelec.*, 2008, **24**, 167.
[48] A. L. Papa, L. Maurizi, D. Vandroux, P. Walker, N. Millot, *J. Phys. Chem. C*, 2011, **115 (39)**, 19012.
[49] C. Mirjolet, A. L. Papa, G. Crehanges, O. Raguin, G. Truc, P. Maingon, N. Millot, *Radioth. Oncol.*, 2013, **108**, 136.
[50] A. L. Papa, L. Dumont, D. Vandroux, N. Millot, *Nanotoxicology*, 2013, **7 (6)**, 1131.
[51] K. S. Brammer, C. J. Frandsen, S. Jin, *Trends in Biotechnology*, 2012, **30 (6)**, 315.
[52] J. Hong, J. Cao, J. Sun, H. Li, H. Chen, M. Wang, *Chem. Phys. Let.*, 2003, **380**, 366.
[53] S. Pavasupree, Y. Suzukia, S. Yoshikawaa, R. Kawahata, *J. Solid State Chem.*, 2005, **178**, 3110.
[54] Y. Lan, X. Gao, H. Zhu, Z. Zheng, T. Yan, F. Wu, S. P. Ringer, D. Song, *Adv. Funct. Mater.*, 2005, **15**, 1310.
[55] C. Pighini, D. Aymes, N. Millot, L. Saviot, *J. Nanopart. Res.*, 2007, **9**, 309.
[56] N. Millot, B. Xin, C. Pighini, D. Aymes, *J. Eur. Ceram. Soc.*, 2005, **25**, 2013.
[57] D. B. Murray, C. H. Netting, L. Saviot, C. Pighini, N. Millot, D. Aymes, H. L. Liu, *J. Nanoelectron. Optoelectron.*, 2006, **1**, 95.
[58] R. F. Egerton, Electron Energy-Loss Spectroscopy in the Microscope, ed. Plenum Press, New-York, 2nd edn, 1996.
[59] M. Wojdyr, *J. Appl. Cryst.*, 2010, **43**, 1126.
[60] D. L. Morgan, H. Y. Zhu, R. L. Frost, E. R. Waclawik, *Chem. Mater.*, 2008, **20(12)**, 3800.
[61] X. Sun, Y. Li, *Chem. Eur. J.*, 2003, **9**, 2229.
[62] Y. Takezawa, H. Imai, *Small*, 2006, **3**, 390.

[63] K. Nakagawa, K. Yamaguchi, K. Yamada, K. I. Sotowa, S. Sugiyama, M. Adachi, Eur. *J. Inorg. Chem.*, 2012, **16**, 2741.
[64] H. Yu, J. Yu, B. Cheng, M. Zhou, *J. Solid State Chem.*, 2006, **179**, 349.
[65] A. I. Ustinov, L. O. Olikhovska, N. M. Budarina, F. Bernard, E. J. Mittemeijer, P. Scardi, Materials Science, ed. Springer Series, 2004.
[66] Y. V. Kolen'ko, K. A. Kovnir, A. I. Gavrilov, A. V. Garshev, J. Frantti, O. I. Lebedev, B. R. Churagulov, O. G. Van Tendeloo, M. Yoshimura, *J. Phys. Chem. B*, 2006, **110**, 4030.
[67] H. Liu, D. Yang, E. R. Waclawik, X. Ke, Z. Zheng, H. Zhu, R. L. Frost, *J. Raman Spectrosc.*, 2010, **41**, 1792.
[68] Y. S. Ponosov, G. A. Bolotin, *Phys. Stat. Sol. B*, 1999, **215**, 137.
[69] Z. Y. Yuan, B. L. Su, *Colloids and Surfaces A: Physico-Chem. Eng. Aspects*, 2004, **241**, 173.
[70] E. Horvath, A. A. Kukovecz, Z. Konya, I. Kiricsi, *Chem. Mater.*, 2007, **19**, 927.
[71] Y. Peng, S. K. Kansal, W. Deng, *Mater. Lett.*, 2009, **63**, 2615.
[72] A. Elsanousi, E. M. Elssfah, J. Zhang, J. Lin, H. S. Song, C. Tang, *J. Phys. Chem. C*, 2007, **111**, 14353.
[73] M. A. Cortes-Jacome, G. Ferrat-Torres, L. F. Flores Ortiz, C. Angeles-Chavez, E. Lopez-Salinas, J. Escobar, M. L. Mosqueira, J. A. Toledo-Antonio, *Catal. Today*, 2007, **126**, 248.
[74] S. Zhang, L. M. Peng, Q. Chen, G. H. Du, G. Dawson, W. Z. Zhou, *Phys. Rev. Lett.* 2003, **91**, 2561031.
[75] D. V. Bavykin, F. C. Walsh, Eur. *J. Inorg. Chem.*, 2009, **8**, 977.
[76] Y. F. Chen, C. Y. Lee, M. Y. Yeng, H. T. Chiu, *Mater. Chem. Phys.*, 2003, **81**, 39.
[77] P. Liu, H. Zhang, H. Liu, Y. Wang, X. Yao, G. Zhu, S. Zhang, H. Zhao, *J. American Chem. Soc.*, 2011, **133 (47)**, 19032.
[78] S. R. Dhakate, N. Chauhan, S. Sharma, R. B. Mathur, *Carbon*, 2011, **49**, 4170.
[79] L. Jiao, X. Wang, G. Diankov, H. Wang, H. Dai, *Nature Nanotech.*, 2010, **5**, 321.
[80] J. Sheng, L. H. Hu, L. Mo, W. X. Li, H. J. Tian, S. Y. Dai, *Sci. China Chem.*, 2012, **55(3)**, 368.
[81] D. V. Bavykin, V. N. Parmon, A. A. Lapkin, F. C. Walsh, *J. Mater. Chem.*, 2004, **14**, 3370.

Graphical Abstract

Multi-step mechanism and integrity of titanate nanoribbons

Vanessa Bellat, Rémi Chassagnon, Olivier Heintz, Lucien Saviot, David Vandroux and Nadine Millot

The structural integrity of titanate nanoribbons has been studied. The original use of several TEM techniques (in particular EFTEM) has proved that their structure is an assembly of smaller ribbons juxtaposed and piled up on one another, leading to superstructures. Moreover, full characterization by other methods (XRD, Raman spectroscopy and XPS) enabled to determine their morphological, structural and chemical characteristics, to better understand their physico-chemical properties and to submit new insights concerning their forming mechanism.